Manuscript submitted to **Biophysical***Journal*
Article

Modelling intermediates of BamA folding an outer membrane protein

Katie M. Kuo[1], David Ryoo[2], Karl Lundquist[3], and James C. Gumbart[1,4,*]

[1]School of Chemistry and Biochemistry, Georgia Institute of Technology, Atlanta GA, 30332, United States
[2]Interdisciplinary Bioengineering Graduate Program, Georgia Institute of Technology, Atlanta GA, 30332, United States
[3]Department of Biological Sciences, Markey Center for Structural Biology, Purdue University, West Lafayette IN, 47907, United States
[4]School of Physics, Georgia Institute of Technology, Atlanta GA, 30332, United States
[*]Correspondence: gumbart@physics.gatech.edu

ABSTRACT

BamA, the core component of the β-barrel assembly machinery (BAM) complex, is an integral outer membrane protein (OMP) in Gram-negative bacteria that catalyzes the folding and insertion of OMPs. A key feature of BamA relevant to its function is a lateral gate between its first and last β-strands. Opening of this lateral gate is one of the first steps in the asymmetric-hybrid-barrel model of BamA function. In this study, multiple hybrid-barrel folding intermediates of BamA and a substrate OMP, EspP, were constructed and simulated to better understand the model's physical consequences. The hybrid-barrel intermediates consisted of the BamA β-barrel and its POTRA5 domain and either one, two, three, four, five, or six β-hairpins of EspP. The simulation results support an asymmetric-hybrid-barrel model in which the BamA N-terminal β-strand forms stronger interactions with the substrate OMP than the C-terminal β-strand. A consistent "B"-shaped conformation of the final folding intermediate was observed, and the shape of the substrate β-barrel within the hybrid matched the shape of the fully folded substrate. Upon further investigation, inward-facing glycines were found at sharp bends within the hybrid and fully folded β-barrels. Together, the data suggest an influence of sequence on shape of the substrate barrel throughout the OMP folding process and of the fully folded OMP.

SIGNIFICANCE

Nearly all outer-membrane proteins (OMPs) in Gram-negative bacteria are β-barrels, yet the precise mechanisms of their insertion into the membrane remain unclear. While it is known that the BAM complex catalyzes insertion, different models have been put forth for how it accomplishes this critical task. Here, using molecular dynamics simulations, we have explored the physical constraints on one such model, in which β-strands of the nascent OMP thread into an opening in the side-wall of BamA, core component of the BAM complex. By modeling and simulating multiple hypothetical intermediate states, we find that BamA is sufficiently labile to accommodate the growing OMP, aided by the presence of glycine residues at sharp bends in its β-barrel.

INTRODUCTION

The outer membrane (OM) of Gram-negative bacteria is an asymmetric bilayer in which numerous integral β-barrel outer-membrane proteins (OMPs) are embedded (1, 2). These proteins carry out a number of necessary functions for the cell, such as transporting nutrients and chemical signals as well as expelling toxins and waste products (3–5). Additionally, there are several proteins involved in building and maintaining the OM itself, including the so-called BAM (β-barrel assembly machinery) complex (6–8). The BAM complex catalyzes the folding and insertion of other OMPs into the OM (9–11). It is composed of BamA, a β-barrel in the OM, and, in *Escherichia coli*, four periplasmic lipoproteins named BamB, BamC, BamD, and BamE (12–16), although the precise constituents can vary by species (8, 11). Regardless, the core component BamA is both essential and universal in Gram-negative bacteria (8, 9, 17, 18) with homologues present in both chloroplasts and mitochondria (19–21).

While the role of the BAM complex in aiding the insertion of OMPs into the OM is known, its precise mechanisms are still unclear. High-resolution structures of the BAM complex have been solved in multiple conformations, exhibiting different states of BamA and indicating its dynamic nature (13–16). In particular, the β1 and β16 strands of the BamA β-barrel are found either anti-parallel to each other in a "closed" conformation or partially separated (22–25). In the latter conformation, the first four β -strands are bent outward while the C-terminal β16 strand kinks inward, leaving the BamA β-barrel partially "open" to the OM (16, 26).

Multiple studies have demonstrated the critical role of

the separation between the BamA β1 and β16 strand (14, 16, 25, 27, 28). This separation is the first step of the so-called "hybrid-barrel model" (also referred to as the "budding model") (22, 29–32). The hybrid-barrel model postulates that the lateral gate created by the separation allows a nascent substrate OMP's C-terminal β-strand to insert between the BamA β1 and β16 strands, using one or both as a template for folding its own β-barrel. The threading model further postulates that nascent OMP β-strands enter BamA's lateral gate sequentially from C- to N-terminus (27). While recent biochemical and structural studies are in agreement with the hybrid-barrel model (26, 31, 33–35), they do not preclude other models as many intermediate steps remain unclear. Recent experiments on BamA coupled to a stalled inserting EspP have been used to propose an asymmetric hybrid barrel as a late-stage intermediate, with several hydrogen bonds maintaining the β-seam interactions between BamA β1 and EspP β12 (34). On the other side of the gate, the BamA β16 strand does not interact as strongly with the EspP β1 strand. This asymmetric hybrid barrel has also been supported through recent structures of hybrid barrel intermediates (26, 31, 35).

Structural and experimental data point towards the hybrid-barrel as the mechanism of BamA function, but many of the intermediate steps and conformational states are still unclear. To resolve the physical plausibility of the hybrid-barrel model, we have built and simulated hybrid-barrel intermediates between BamA and a substrate OMP, the 12-stranded type Va autotransporter EspP. There are six initial folding intermediates modeled here with either two, four, six, eight, ten, or twelve β-strands of EspP. The dynamics and structural characteristics are explored in these models and simulations. We find that the hybrid-barrel intermediates are asymmetric, with the substrate EspP becoming more circular as the number of β-hairpins increases. The intermediates with six β-hairpins of EspP were consistently observed in a "B" conformation of the two β-barrels. This finding is in contrast to the "8" shape observed in a high-resolution structure of the BAM complex folding a substrate BamA (31). The simulation results further suggest that the sequence of the substrate has an influence over the shape of the fully folded OMP.

METHODS

System construction

Eight systems in total were built in this study. To investigate the intermediates of hybrid-barrel folding, we built six folding intermediates of EspP with the BamA β-barrel (residues 424-810) and the POTRA5 domain (P5; residues 347-423) from *E. coli*. These intermediates had either one, two, three, four, five, or six β-hairpins of EspP (PDB ID: 3SLJ) within the BamA lateral gate (36). The systems with 1 to 6 β-hairpins were based off of a cryo-electron microscopy structure of the BAM complex, with BamA in a laterally open conformation (PDB ID: 5LJO) (16). These first six structures are identified as BamA-EspP(*n*), where *n* is a number between 1 and 6. An additional folding intermediate with all six β-hairpins of EspP and the entire BAM complex was also built, labeled as BAM-EspP in this study. The eighth and final system is the full BAM complex folding a substrate BamA β-barrel (PDB ID: 6V05) (31). The BamA-EspP(1), BamA-EspP(2), BamA-EspP(3), and BamA-EspP(4) systems were built following one protocol (Table S2) while the BamA-EspP(5), BamA-EspP(6), BAM-EspP, and BAM-BamA systems were built using a different protocol (Table S3). The specific protocols are further elaborated on in the sections below.

The systems studied were all built using CHARMM-GUI (37, 38). Every system and simulation in this study used a realistic *E. coli* OM. The outer leaflet was K12 Type 1 *E. coli* rough LPS with lipid A, R1 core, and no O-antigens. The lipid A was neutralized with Ca^{2+} ions and the R1 core with Mg^{2+} ions. The inner leaflet was composed of a ratio of 15:4:1 PPPE, PVPG, and PVCL2 lipids (39). The system was solvated with TIP3P water (40) and 0.15 M KCl was added. Each system was built with different *x* and *y* dimensions to accommodate the size of the growing hybrid barrel.

Iterative opening at the BamA lateral gate

The first step in building the BamA-EspP hybrid barrels was to separate the β1 and β16 strands of BamA until there is enough space to accommodate the width of one β-hairpin. To increase the distance between the lateral gate strands in a minimally pertubative manner, a one-sided harmonic restraint (100 kcal/mol·Å^2) on the distance between the β1 and β16 strands was imposed, which prevented the distance from going below whatever it was at the start of the simulation. After the first run, the maximum distance spontaneously achieved between the lateral-gate strands was determined, with the corresponding conformation used to seed the next run. This distance was also set as the harmonic restraint minimum distance for the next run. This process was repeated until there was sufficient space between the BamA β1 and β16 strands to accommodate one β-hairpin. For these systems, the process was applied around 10-20 times to generate enough separation. Specific run times and the number of runs are detailed in Table S4.

Building the hybrid-barrel intermediates for BamA-EspP(*n*)

The hybrid barrel intermediate with the BamA β-barrel plus the P5 domain and one β-hairpin of EspP was built by separating the lateral gate using the iterative opening method described above and then inserting the EspP β-strands within the gate. Two key features of β-barrels were used to determine the register of the EspP β-strands with respect to BamA β1 and β16. The first feature is the alternating polar and nonpolar residues along the β-strand where the β-barrel resides in the OM, excluding periplasmic domains and extracellular loops

(41). The second feature is the aromatic girdles that cap the β-barrel at its top and bottom (Fig. S1). The aromatic girdle is composed of outward-facing aromatic residues where the β-barrel interfaces with the edges of the hydrophobic core of the outer and inner leaflets of the membrane (42). Using these features, the EspP β12 and β11 strands were aligned within BamA β1 and β16, respectively, to construct BamA-EspP(1).

The intermediate of BamA-EspP with two β-hairpins, BamA-EspP(2), was built in a similar fashion to BamA-EspP(1) (Table S2). The BamA β1 and β16 strands were separated using the iterative lateral gate opening method until enough space was created to accommodate two β-hairpins of EspP. The β12 and β9 strands of EspP were aligned with BamA β1 and β16, respectively, matching the alternating non-polar residues and the aromatic girdles of both β-barrels.

BamA-EspP(3) was built by separating the BamA-β16 seam from the adjacent EspP β-strand in BamA-EspP(2) using the iterative opening method until there was enough space at the β-seam for the third β-hairpin. The same considerations of the aromatic girdles was followed to determine the register of the third β-hairpin with BamA β16. This method was also followed to build BamA-EspP(4), creating separation at the BamA-β16 seam of BamA-EspP(3) until there was enough for the fourth β-hairpin of EspP (Table S2). Determining the sufficient degree of separation at the BamA β16 strand to add a β-hairpin within the space for BamA-EspP(1), BamA-EspP(2), BamA-EspP(3), and BamA-EspP(4) was done through trial and error with each additional β-hairpin. Hydrogen-bond restraints used to equilibrate the resulting hybrid structures are described below.

The BamA-EspP(5) and BamA-EspP(6) intermediates were modeled from the BAM-EspP hybrid barrel described below, where the hydrogen-bond restraints were applied at the β-seams between BamA and EspP. From the BAM-EspP intermediate, the β-barrel and P5 domain of BamA were retained along with the substrate EspP. For BamA-EspP(6), all strands of EspP were retained. For BamA-EspP(5), only five β-hairpins of EspP were kept for the model (Table S3), and the gap was closed with hydrogen-bond restraints between adjacent β-strands.

Building the hybrid-barrel intermediate for BAM-EspP

To build the hybrid barrel intermediate for BAM-EspP, the full BAM complex (PDB ID: 5LJO) (16) and EspP (PDB ID: 3SLJ) (36) structures were positioned close to each other. The position of EspP relative to the BAM complex was based on the previously identified photo-crosslinks, where residues F1300, F1113, and F1214 of the EspP β-barrel were found to be close to BamA, BamB, and BamD, respectively (43). Then, using distance restraints between the respective first and last β-strands of each β-barrel, BamA and EspP were forcibly opened laterally to a separation of ~30 Å, measured from the Cα atoms. Next, hydrogen-bond restraints were applied to β1 of BamA and β12 of EspP as well as to β16 of BamA and β1 of EspP, aligned based on the two features noted above, namely matching the polar/nonpolar residues as well as the aromatic girdles. These hydrogen bonds at the β-seams were enforced for 100 ns.

To refine the resulting BAM-EspP hybrid-barrel construct, we also used targeted molecular dynamics (TMD) with the cryo-EM BAM-BamA hybrid structure (PDB ID: 6V05) (31) as a reference. This experimentally determined structure shows the BAM complex (BamA machine) folding and inserting another copy of BamA (BamA substrate). BamA machine of the BAM-BamA hybrid structure was aligned to BamA of the merged BAM-EspP hybrid model, and the first two β-strands and last two β-strands of the BamA substrate of the BAM-BamA hybrid structure were aligned to those of EspP of the BAM-EspP hybrid intermediate. However, since the β1 and β2 strands of the BamA substrate are missing in the BAM-BamA hybrid structure, we aligned the β3 and β4 strands of the BamA substrate structure to the first two β-strands of the modeled EspP barrel. The RMSD of the targeted atoms at the start of TMD was 2.13 Å and the final RMSD was 1.38 Å, giving a rate of 0.0075 Å/ns of change over the 100-ns simulation. The resulting conformation was restrained for 100 ns, followed by an additional 100 ns with only the first two β-strands and last two β-strands of BamA and EspP respectively restrained. Finally, the secondary structure and the hydrogen bonds of the whole structure were maintained for 350 ns (see Fig. S2 for RMSD of BamA during and after the fitting process). The resulting BAM-EspP model was used for simulations as well as to create the BamA-EspP(5) and BamA-EspP(6) systems.

Building the hybrid-barrel intermediate for BAM-BamA

To build the BAM-BamA hybrid-barrel system, we started from the previously identified structure (PDB ID: 6V05) (31). As the original PDB structure was missing several parts of the BAM complex, we also had to align and combine those missing parts from other published structures (PDB IDs: 5D0O, 5D0Q) (14). For the lipoproteins BamB, BamC, BamD, and BamE, we lipidated their N-terminal cysteines and anchored the three acyl chains on each in the inner leaflet of the OM. However, we did not add the missing β1 and β2 strands of the BamA substrate.

Molecular dynamics simulations

Each system went through multiple stages of equilibration. In the first stage, we restrained the entire system except the lipid tails for 0.5 ns. In the second stage, we restrained the proteins and allowed the rest of the system to equilibrate for 1 ns. In the third stage, we restrained just the protein backbone for 1 ns. Following these stages, everything in the system was released and allowed to equilibrate for 10 ns with secondary structure

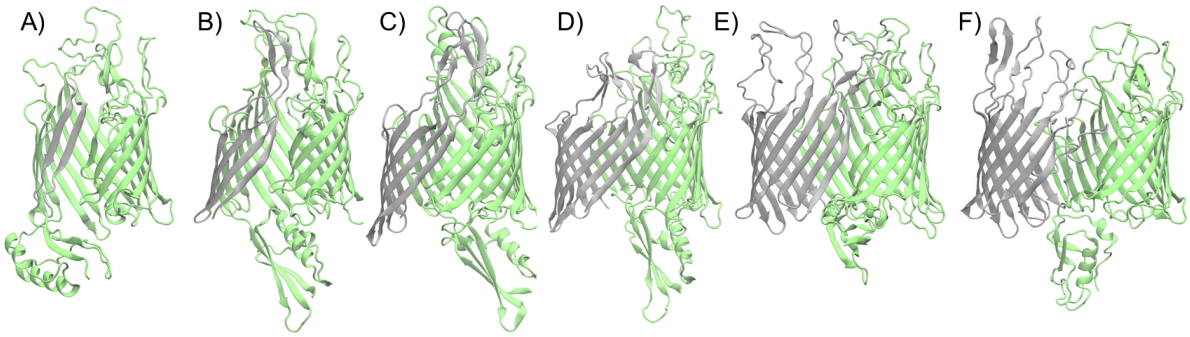

Figure 1: BamA (green)-EspP (grey) hybrid barrels modeled. Snapshots are taken from the end of a 2-µs equilibrium simulation (A-E) or 5-µs simulation (F), with the focus on the separation between EspP and BamA's β16 strand. The images show (A) 1 β-hairpin of EspP (BamA-EspP(1)), (B) 2 β-hairpins (BamA-EspP(2)), (C) 3 β-hairpins (BamA-EspP(3)), (D) 4 β-hairpins (BamA-EspP(4)), (E) 5 β-hairpins (BamA-EspP(5)), and (F) 6 β-hairpins (BamA-EspP(6)).

restraints (ssrestraints) applied. The ssrestraints maintain the dihedral angles and backbone hydrogen bonds while allowing side chains to move freely.

Simulations were run at a constant temperature of 310 K using Langevin dynamics and at constant pressure using the anisotropic Langevin piston barostat (44). Long-range interactions were evaluated using the Particle-Mesh Ewald (PME) method (45), while a 12 Å cutoff was used for van der Waals interactions with a force-switching function beginning at 10 Å. The CHARMM36m force field for proteins (46) and the CHARMM36 force field for lipids (47) were used.

For the BamA-EspP hybrid barrels, we used collective variables (colvars) in NAMD to maintain hydrogen bonds at the seams between BamA and EspP (48, 49) for 100 ns with ssrestraints applied. After this stage, the hydrogen-bond colvars and ssrestraints were released and the system was allowed to equilibrate for 15 ns. While equilibration stages used a 2-fs timestep, all subsequent simulations used hydrogen mass repartitioning (HMR) along with a timestep of 4 fs (50, 51) and were run using AMBER (52). For each hybrid barrel system built, two replicas were run where the initial positions were the same but the initial velocities were randomized. Further divergence occurs due to the Langevin thermostat, which uses a different random seed for each simulation. The total simulation time across all the different systems and replicas is 38 µs. Reduced simulation trajectories have been made available at DOI: 10.5281/zenodo.6785311.

Analysis of simulations

Hydrogen bond measurements were done using VMD (53) with a distance cutoff of 3.5 Å and angle cutoff of 30° (measured as Acceptor-Donor-Hydrogen). The number of hydrogen bonds between the backbones of neighboring BamA and EspP β-strands were measured and then averaged over the trajectory. The distance between the center of mass of the backbones of neighboring β-strands at each β-seam was also measured and averaged over the total trajectory. Shape measurements (54) were done following previous protocols. The shape measurement first determines the position of the C_α atoms in the β-barrel. Using the cv2 python library and cv2.fitEllipse function, the coordinates were flattened onto the membrane plane, and an ellipse was fit to them. The semi-major (a) and semi-minor (b) axes of the fitted ellipse were calculated and the ratio of the semi-minor to semi-major (b/a) was taken. A shape value of 1 indicates a perfect circle, while lower values indicate a flatter shape.

The dynamics at the β-seams were further quantified by first taking the angle between the first principal axes of the neighboring two BamA and two EspP β-strands. Additionally, the angle of the P5 domain with respect to the BamA β-barrel was measured (39). The rotation angle of the periplasmic domains of the BAM complex, BamB, BamC, BamD, and BamE, was also quantified following our previous study (26).

RESULTS

Hybrid-barrel intermediates are typically asymmetric

Hybrid barrels between BamA and increasing numbers of EspP β-strands were constructed sequentially. For hybrid barrels with between 1 and 4 β-hairpins of EspP, denoted BamA-EspP(1) through BamA-EspP(4), an iterative opening approach for BamA was used. In this approach, opening of BamA's lateral gate was captured in equilibrium simulations and then allowed to progressively increase by preventing any reduction in gate-opening distance. After a sufficient opening was captured for each system, an additional β-hairpin of EspP was inserted. For hybrid barrels with 5 or 6 β-hairpins of EspP, systems were initially modeled based on the BAM-BamA cryo-EM structure (31). See Methods for more details on both approaches. The BamA-EspP intermediates had hydrogen-bond colvars maintained at the β-seams for 100 ns before they were equilibrated for 2 µs in duplicate. The BamA-EspP 6β-hairpin intermediate was run for 5 µs in duplicate to observe the long-scale dynamics of the system.

One feature of particular interest in the intermediates is the seams between BamA and the adjacent EspP β-strand. The

first β-seam is between BamA β1 and EspP β12, while the second is between BamA β16 and the current N-terminal EspP β-strand (between β11 and β1). Among the six hybrid barrel intermediates, frequent separation was observed between BamA β16 and EspP (Fig. 1). When quantifying the degree of interaction at each β-seam, the BamA β1 strand interacted with the EspP β12 strand consistently via 3-5 hydrogen bonds (Fig. 2A). At the BamA-β16 seam, the variability of its interaction with EspP is reflected in the inconsistent number of hydrogen bonds (Fig. 2B).

In the simulations of BamA-EspP(1), one replica exhibits an opening at the BamA-β16 seam while in the second replica, this β-seam remained closed, quantified via the average number of hydrogen bonds between the backbones of the β-strands (Fig. 2B). Similar to the replicas for BamA-EspP(1), BamA-EspP(2) showed one replica with the BamA-β16 seam open and the other with it at least partially closed.

While both closed and open conformations were observed at the β-seam with BamA β16 for BamA-EspP(1) and BamA-EspP(2), the conformation of the β16 strand was consistent for both replicas for BamA-EspP(3), BamA-EspP(4), BamA-EspP(5), and BamA-EspP(6). BamA-EspP(3) maintained 4-5 hydrogen bonds at both β-seams, keeping the lateral gate closed (Fig. 2B). It is important to note that the interactions between the β-strands of BamA and EspP are facilitated by interactions between the extracellular loops (Fig. S3). In contrast, BamA-EspP(4), BamA-EspP(5), and BamA-EspP(6) are asymmetric with a closed seam at BamA β1 and a more open seam at BamA β16. These intermediates have 4-5 hydrogen bonds between BamA β1 and EspP β12 in both replicas (Fig. 2A). However, there are 0-2 hydrogen bonds between the BamA β16 strand and the EspP β-strand, meaning the BamA-β16 seam remains open in these intermediates (Fig. 2B).

The hydrogen-bond results are further supported by the distance between BamA and EspP β-strands at the BamA-β1 and -β16 seams (Fig. S4). The distances between the β-strands at BamA β1 (Fig. S4A) are lower compared to the distances at BamA β16 (Fig. S4B). Consistent with the asymmetric-hybrid-barrel model, the BamA β16 strand does not form stable and consistent hydrogen bonds with EspP in most intermediate states, which results in a larger strand-separation distance.

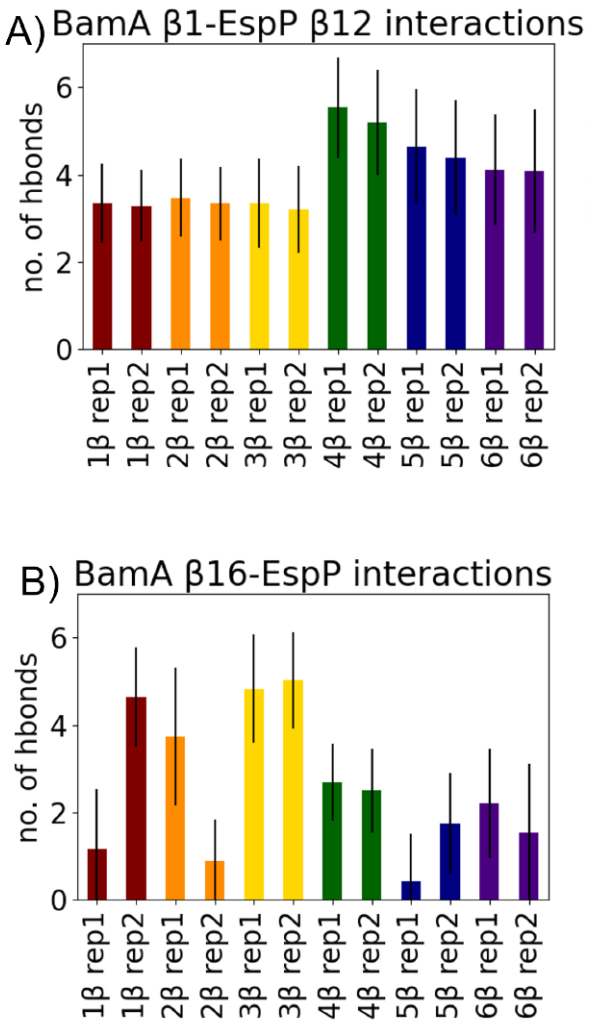

Figure 2: Hydrogen bonds between the backbones of the β-seams, measured for each BamA-EspP hybrid-barrel intermediate and replica. (A) BamA β1 and EspP β12. (B) BamA β16 and the adjacent EspP β-strand. The solid colored bar is the average over 2 µs (5 µs in the case of BamA-EspP(6)) and the black line represents the standard deviation.

The shape of the substrate in the hybrid barrel is determined by its final folded state

When observing the different conformations of the hybrid-barrel intermediates, the equilibrated conformations of BamA-EspP(2), BamA-EspP(3), BamA-EspP(4), and BamA-EspP(5) evolve from an oval shape towards a heart shape (Fig. 3). The cleft of the heart is at the BamA-β16 seam, which bends inward. Interestingly, BamA-EspP(6) displays a more dramatically altered conformation, a "B" shape when viewed from the extracellular side (Fig. 3). As the simulation progressed, both replicas underwent conformational changes from an oval shape to this distinct "B" shape, where there is a inward-cleft at BamA β16 but the BamA β1 side is flat.

To explore these changes in overall hybrid-barrel conformations as well as in BamA and EspP separately, we quantified the shapes of each. Here, the shape is defined as the ratio of the semi-minor axis to the semi-major axis of the ellipse fit to the C_α atoms flattened onto a plane (54). A value of 1 (the maximum) for the shape indicates that the β-barrel (or hybrid barrel) is circular, while the lower the value of the shape (minimum of 0), the flatter it is (54). Visually, the shift from an oval conformation to something else is most extreme in BamA-EspP(6), where it forms a "B" shape. This conformation exhibits a cleft at the BamA β16 but none at BamA β1. We also see changes in the oval shape to a heart

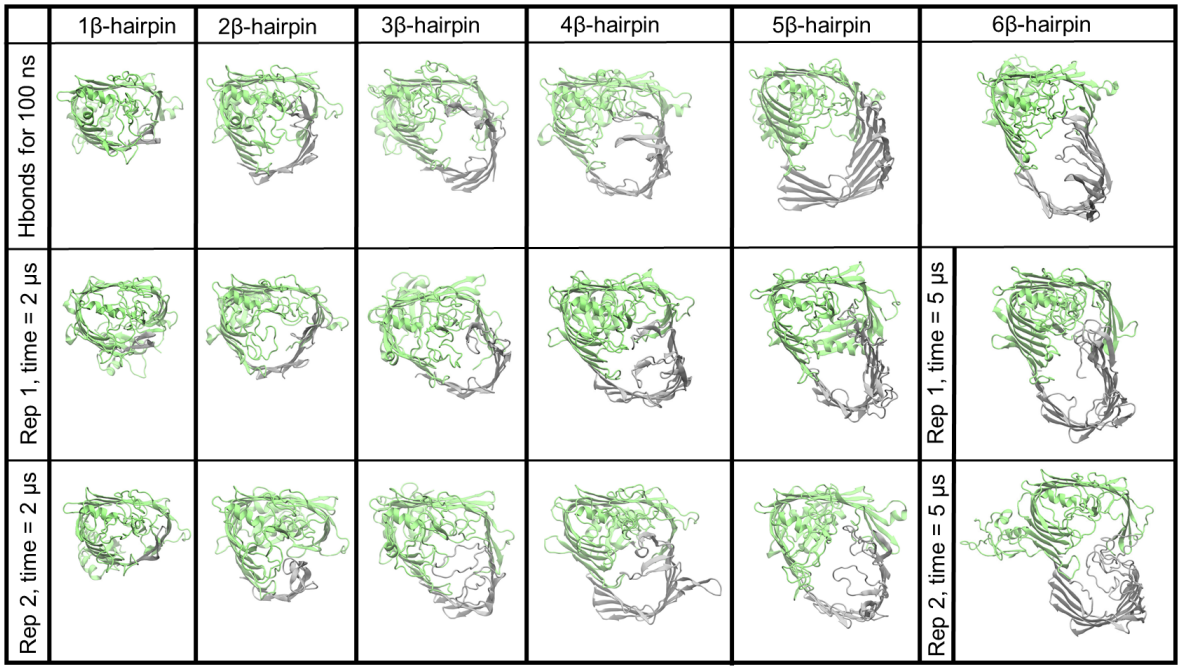

Figure 3: Hybrid-barrel intermediates as viewed from the extracellular side. (top) After 100 ns with inter-strand hydrogen bond colvars. (middle) Replica 1 at the end of equilibrium simulations. (bottom) Replica 2 at the end of equilibrium simulations. Viewpoint highlights the cleft formed at the BamA β16 strand in intermediates.

shape for the intermediates with fewer β-hairpins. However, after quantification, there is no obvious trend in the values for the shape of the hybrid barrel of BamA-EspP nor in those for the shape of BamA itself (Fig. S5).

When looking more closely at the shape of only the EspP substrate in the hybrid-barrel intermediates, a general trend is seen in which the shape value increases as the number of β-hairpins in the hybrid barrel increases. From BamA-EspP(2) to BamA-EspP(6), the shape of EspP begins relatively flat, becoming more circular as the number of β-hairpins of the EspP β-barrel increases. The shape of EspP in BamA-EspP(6) most closely matches the shape of the fully folded EspP substrate alone (0.75-0.83) (Fig. 4). At each intermediate state, the fluctuations encompass the shape of the fully folded substrate (Fig. S6). As the substrate grows in β-hairpins, the average shape approaches the fully folded state and its final value. This observation also holds true for the hybrid barrel of the full BAM complex with six β-hairpins of EspP inserted (BAM-EspP).

We compared our BamA-EspP and BAM-EspP hybrid-barrel intermediates to our equilibrium simulations of a recently published structure of the BAM complex folding a BamA-substrate (PDB ID: 6V05 (31)), labeled as BAM-BamA. The BamA in the complex that is folding the substrate is referred to as BamA-machine while the BamA being folded is BamA-substrate. In both replicas of this hybrid intermediate, BamA-substrate is similar in shape to a fully folded BamA. Looking at the BAM-BamA hybrid barrel from above,

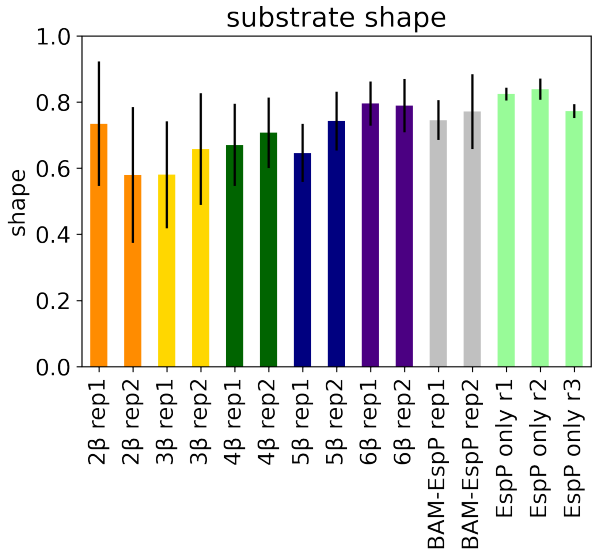

Figure 4: Shapes of EspP in a hybrid barrel or alone (1 is circular and 0 is completely flat). Shapes for EspP in each of the two replicas of hybrid barrels BamA-EspP(2) through BamA-EspP(6) are shown, along with those for EspP in the full BAM-EspP complex. Finally, for comparison, shapes for three replicas of the mature EspP membrane domain alone are shown. BamA-EspP(1) is not included due to the low number of β-hairpins. As the hybrid barrel increases in the number of substrate β-hairpins, the shape of the substrate approaches the shape of EspP when fully folded.

an apparent "8"-shaped conformation of the hybrid-barrel is maintained throughout the simulation for both replicas (Fig. 5B). The cleft at the BamA-β1 seam is present throughout the simulation, and more dramatically at the BamA β16 strand. Even though the hybrid barrel is in a different conformation with BamA-substrate compared to with EspP, the shape of BamA-substrate closely matches its shape when fully folded (Fig. S7C). This observation aligns with the previous finding that the shape of EspP in BamA-EspP(6) is close to its shape when fully folded. When comparing the BAM-BamA and BAM-EspP simulations, it is interesting to note that the BAM-EspP system also starts in the "8"-shaped conformation but shifts to the "B"-shaped conformation over the course of the simulation (Fig. 5A).

Inward-facing glycines found at the turns of the final hybrid-barrel intermediate and those of fully folded substrates

The shape of the substrate in the hybrid barrel becomes increasingly like a circle while it reaches the shape of the fully folded substrate. This finding suggests a possible role for sequence of the β-barrel on its final shape. Upon inspection of BamA and the EspP substrate within the hybrid barrel, glycines were found at specific locations of each β-barrel. In particular, within the BamA β-barrel, inward-facing glycines were found at both turns of the barrel (highlighted in purple in Fig. 6). The glycines at these turns of BamA are between 57% and 97% conserved across nearly 2600 species (Table S1). Within the EspP substrate, inward-facing glycines were also found at the turns of the substrate within the hybrid barrel (green and yellow in Fig. 6B) as well as the fully folded β-barrel (green and red in Fig. 6D). Interestingly, in the BAM-BamA hybrid barrel, glycines were also found located at additional turns of BamA-substrate (Fig. S7). The location of glycines at the turns suggests that the glycines within the sequence of the β-barrel help to determine the final shape of the folded substrate during the hybrid-barrel assembly process.

The observations of glycines at the turns of β-barrels and the resulting shape are supported by a previous computational study (54). Analyzing the 119 available structures of OMPs at the time, a correlation between glycines facing the interior of a β-barrel and its shape was found. The presence of these glycines resulted in a sharper turn within the β-barrel, with more glycines found in β-barrels with fewer strands due to the sharper turns necessary compared to β-barrels with more strands. Here, we find that the "B" versus the "8" shape of the hybrid barrel corresponds to the substrate, with EspP associated with a "B" shape and BamA-substrate with a "8" shape. The "B" shape is distinguished by the strands at the BamA-β1 seam lying in the same plane while the strands at the BamA-β16 seam formed a cleft. This finding indicates that not only does the substrate sequence have an influence on the final shape of the substrate, but also that the substrate itself can influence the conformation of BamA in the hybrid barrel.

Distinct features in hybrid barrels with the full BAM complex

The hybrid barrels with the full BAM complex are observed in either the "B" or "8" shape depending on the substrate. Examining the β-seams between the BamA-machine and substrate barrels, the angles between the first principal axes of the two adjacent β-strands on either side of each seam were measured. The angles at the BamA-β16 seam are higher in comparison to those at the BamA-β1 seam (Fig. 7) in both the full complex hybrid barrels and the BamA-EspP(*n*) intermediates. The BamA β16 and EspP β1 strands are at an angle of 123-127° in the full complex hybrid barrel (Fig. 7B), while the BamA-machine β16 and BamA-substrate β1 strands are at a 110-175° angle to each other. In the "8"-shaped BAM-BamA complex, the β-strands can range from an obtuse angle to a nearly straight one. For the "B"-shaped BAM-EspP complex, they are consistently at an obtuse angle to each other. For BAM-EspP in particular, the "B"-shaped hybrid barrel has a much higher angle at the BamA-β16 seam compared to the BamA-EspP(*n*) intermediates.

The BAM-EspP and BAM-BamA hybrid barrels are further distinguished from BamA-EspP(*n*) by the angle between the P5 domain and the BamA β-barrel. In the majority BamA-EspP(*n*) systems, which only include the BamA β-barrel and P5 domain, the P5 domain angle ranges from 20-35° to the BamA β-barrel (Fig. S8A). However, in the hybrid barrels with the full BAM complex, the P5 domain angle is 80-85° in BAM-EspP and 92-97° in BAM-BamA. BamD within the BAM complex interacts with the P5 domain (Fig. S9B,C), affecting its angle. More specifically, BamD interacts with BamA P5 at D358 and T359.

In both the BAM-EspP and BAM-BamA systems, the BamA-machine β16 strand is separated from the adjacent substrate β-strand. The lateral gate is effectively open with the P5 domain occluding the BamA β-barrel from the periplasmic side, as expected. However the rotation angle of the periplasmic domains of the complex (BamB, BamC, BamD, and BamE) is closer to what has been previously found for the BAM complex in a laterally closed conformation. In previous work, the rotation angle of the BamB-BamE fluctuates around 60° in the BAM complex with an open lateral gate and 0° with a closed lateral gate (26). In the hybrid barrels with the full BAM complex simulated here, the lateral gate is open but the rotation of BamB-BamE fluctuates around 0° (Fig. S8), closer to the rotation angle of the closed BAM complex in our previous simulations. This shift in the rotation angle of the periplasmic domains suggests a further unidentified role of BamB-BamE during hybrid-barrel folding.

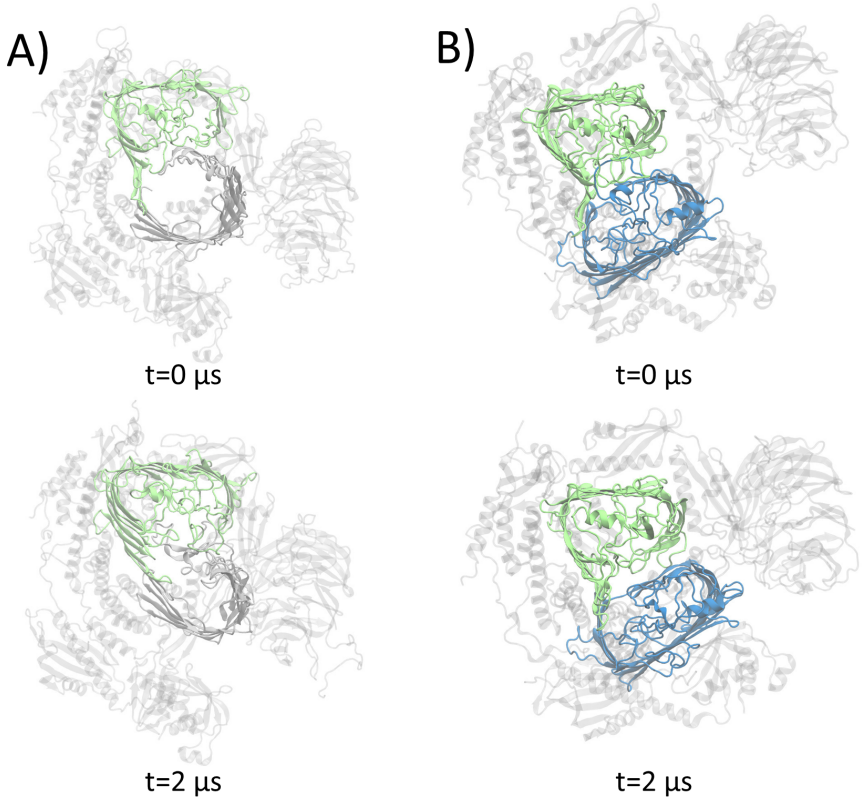

Figure 5: Hybrid intermediates of the BAM complex. (A) BAM-EspP hybrid-barrel intermediate at time t = 0 μs and the end conformation at t = 2 μs. Shown are BamA (green), the rest of the BAM complex (transparent) and EspP (grey). (B) BAM-BamA hybrid-barrel intermediate at t = 0 μs and t = 2 μs. Shown are BamA-machine (green), the rest of the BAM complex (transparent), and the BamA-substrate (blue). Both BAM-EspP and BAM-BamA hybrid-barrel intermediates begin the simulation at t = 0 μs in the "8"-shaped conformation. The "8"-shaped conformation is maintained for BAM-BamA, but BAM-EspP shifts to a "B"-shaped conformation by the end of t = 2 μs.

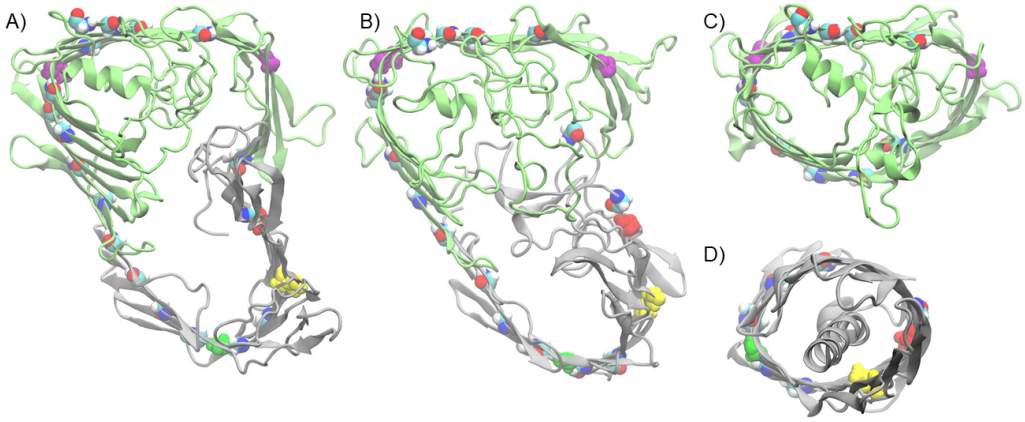

Figure 6: Inward-facing glycines highlighted in van der Waals representation. Specific glycines at the turns of the β-barrels are colored purple for BamA and red, yellow, and green for EspP. (A) BamA-EspP(6). (B) BAM-EspP. (C) BamA in the BAM complex. (D) EspP alone. The purple glycines in BamA are consistently at the turns of the β-barrel. The green glycines in EspP are also at the turns of the hybrid-barrel and fully folded substrate β-barrel, while the yellow glycines are only at the turns in the hybrid barrel and the red only at the turns in the fully folded BamA.

DISCUSSION

In this study, the possible progressive states of OMP folding via sequential hybrid-barrel intermediates were constructed and simulated to observe their characteristics and physical plausability. Systems of the BamA β-barrel and its P5 domain with one to six β-hairpins of EspP were first simulated (BamA-

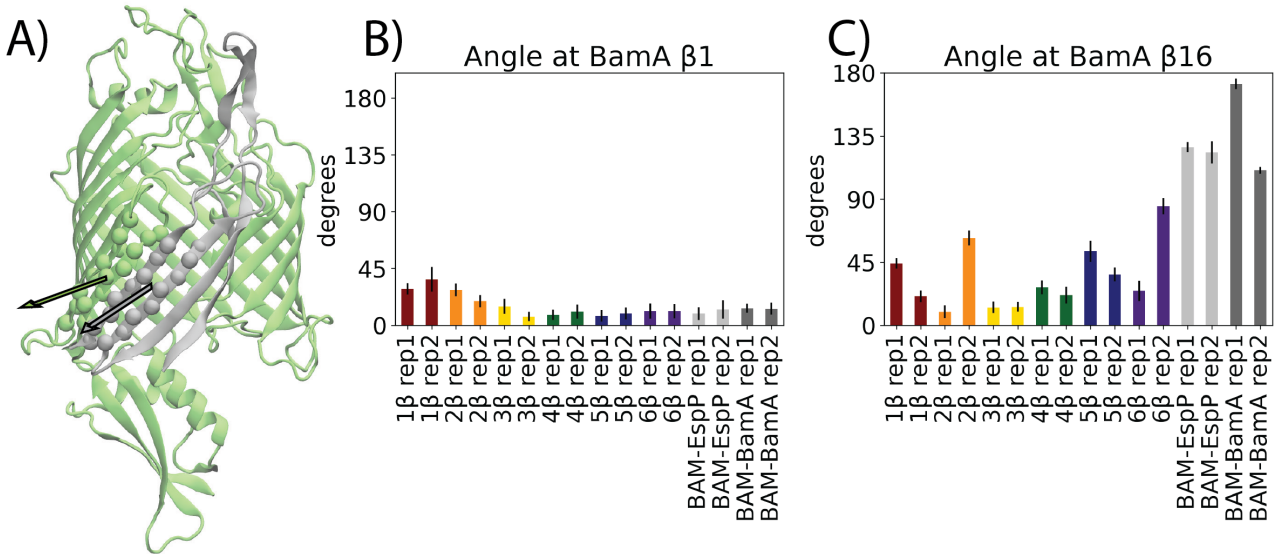

Figure 7: Angles between normal vectors of the adjacent β-strands at the two seams. (A) Representative conformation from BamA-EspP(2) illustrating the two normal vectors. (B,C) Measured angle at the (B) BamA-β1 seam and (C) BamA-β16 seam. See Figs. S10, S11 for the angles versus time. This measurement demonstrates in part the influence of the inward-facing kink of the BamA β16 (28).

EspP(1) through BamA-EspP(6)). Within these BamA-EspP intermediates, a greater number of hydrogen bonds were typically observed between the proteins' backbones at the BamA-β1 seam compared to the BamA-β16 seam. Additionally, systems of the final hybrid barrel intermediate with the full BAM complex and the substrate EspP (BAM-EspP) or BamA (BAM-BamA) were constructed and simulated.

In the hybrid-barrel intermediates constructed here, the BamA and substrate β-strands at both junctions, that with BamA β1 and that with BamA β16, were initially fully hydrogen bonded along their respective backbones. However, over time, the simulations revealed the BamA β16 side to be more dynamic, possessing fewer hydrogen bonds than the β1 side in most simulations (Fig. 2). These results broadly support the asymmetric hybrid barrel model, which is based on disulfide-bond crosslinking (34) as well as recently published cryo-EM structures (31, 35). In the crosslinking experiments, BamA β1 and EspP β12 form stable interactions while BamA β16 does not interact as strongly with EspP β12 (34). The decreased stability of the seam between the substrate and BamA β16 has now been observed in biochemical assays, high-resolution structures, and our simulations.

Considering the shape of the hybrid-barrel intermediates, as the number of β-hairpins increases in the hybrid barrel, the substrate EspP becomes more circular, approaching its shape when fully folded and separated from BamA. Additionally, when looking at the final hybrid-barrel intermediates, BamA-EspP(6) and BAM-EspP, there is a consistent "B" shape in which the BamA β1 side of the hybrid barrel is flat while the BamA β16 side curves inwards. Notably, the BAM-EspP simulation starts in a "8" shape and gradually transitions to the "B" shape (Fig. 5). The BAM-BamA system, in contrast, starts in the "8" shape and maintains this conformation throughout the simulation. We also found that the turns of the β-barrels of both BamA and EspP contain inward-facing glycines, many of which are moderately to highly conserved (Table S1), suggesting they play a role in the folding and shape of OMPs. This finding is in agreement with previous work that found glycines are predominantly located in sharp turns of OMPs (54). When combined with the different shapes observed for hybrids with EspP or a BamA substrate, a role for sequence in hybrid-barrel shape as well as the fully folded shape becomes apparent.

The hybrid barrels built with the full BAM complex have a couple of unique features that were characterized. In particular, the angle between the BamA-machine β16 and adjacent substrate strand were 110-175° to each other in the systems with the full BAM complex. These β-strands at the lateral gate were separated from each other, leaving the gate open with the P5 domain occluding the BamA β-barrel. While the P5 domain being perpendicular to the β-barrel was expected, what was not expected was that the rotation angle of the periplasmic domains is ~0° in both BAM-EspP and BAM-BamA (Fig. S8). This is in contrast to our previously reported work (26), where simulations of just the BAM complex in the laterally closed state showed the periplasmic domains rotation at around 0° as well. Thus, the rotation of the periplasmic domains in the hybrid barrels towards the end of OMP folding more closely matches the rotation in a closed BAM complex.

There are several theories, models, and hypotheses about how the BAM complex functions (27, 35, 55, 56). In our study, by modeling specific intermediate states, we find support

for the asymmetric hybrid-barrel model. Furthermore, our simulations demonstrate that BamA is sufficiently labile to interface with substrate intermediates of between 2 and (at least) 12 β-strands. The threading model, which is an extension of the hybrid-barrel model, states that the unfolded substrate OMP is transferred from the periplasm to the open lateral gate 1-2 β-strands at a time, utilizing BamA's β1 and β16 strands as a scaffold to fold the substrate. Our simulations do not address how the substrate OMP is threaded nor the transition between the unfolded and folded states, but they do demonstrate the physical plausibility of the threaded intermediates. Recent cryo-EM structures of insertion intermediates have been interpreted as support for (26) or against (35) the threading model; more data are needed to resolve this debate.

AUTHOR CONTRIBUTIONS

K.M.K., D.R., and K.L. performed research and analyzed data. All authors wrote the paper.

ACKNOWLEDGEMENTS

This work was supported by the National Institutes of Health (R01-GM123169) and the Department of Education Graduate Assistance in Areas of National Need (GAANN) program at the Georgia Institute of Technology (GT; P200A210014). Computational resources were provided through the Extreme Science and Engineering Discovery Environment (XSEDE; TG-MCB130173), which is supported by the National Science Foundation (NSF; ACI-1548562). This work also used the Hive cluster, which is supported by the NSF (1828187) and is managed by the Partnership for an Advanced Computing Environment (PACE) at GT.

DECLARATION OF INTERESTS

The authors declare no competing interests.

REFERENCES

1. Schiffrin, B., D. J. Brockwell, and S. E. Radford, 2017. Outer membrane protein folding from an energy landscape perspective. *BMC Biol.* 15:123.

2. Horne, J. E., D. J. Brockwell, and S. E. Radford, 2020. Role of the lipid bilayer in outer membrane protein folding in Gram-negative bacteria. *J. Biol. Chem.* 295:10340–10367.

3. Koebnik, R., K. P. Locher, and P. Van Gelder, 2000. Structure and function of bacterial outer membrane proteins: barrels in a nutshell. *Mol. Microbiol.* 37:239–253.

4. Wimley, W. C., 2003. The versatile beta-barrel membrane protein. *Curr. Opin. Struct. Biol.* 13:404–411.

5. Fairman, J. W., N. Noinaj, and S. K. Buchanan, 2011. The structural biology of β-barrel membrane proteins: a summary of recent reports. *Curr. Opin. Struct. Biol.* 21:523–531.

6. Nikaido, H., 2003. Molecular basis of bacterial outer membrane permeability revisited. *Microbiol. Mol. Biol. Rev.* 67:593–656.

7. Hagan, C. L., T. J. Silhavy, and D. Kahne, 2011. β-Barrel membrane protein assembly by the Bam complex. *Annu. Rev. Biochem.* 80:189–210.

8. Webb, C. T., E. Heinz, and T. Lithgow, 2012. Evolution of the β-barrel assembly machinery. *Trends Microbiol.* 20:612–620.

9. Voulhoux, R., M. P. Bos, J. Geurtsen, M. Mols, and J. Tommassen, 2003. Role of a highly conserved bacterial protein in outer membrane protein assembly. *Science* 299:262–265.

10. Wu, T., J. Malinverni, N. Ruiz, S. Kim, T. J. Silhavy, and D. Kahne, 2005. Identification of a multicomponent complex required for outer membrane biogenesis in *Escherichia coli*. *Cell* 121:235–245.

11. Noinaj, N., J. C. Gumbart, and S. K. Buchanan, 2017. The β-barrel assembly machinery in motion. *Nat. Rev. Microbiol.* 15:197–204.

12. Hagan, C. L., S. Kim, and D. Kahne, 2010. Reconstitution of outer membrane protein assembly from purified components. *Science* 328:890–892.

13. Bakelar, J., S. K. Buchanan, and N. Noinaj, 2016. The structure of the β-barrel assembly machinery complex. *Science* 351:180–186.

14. Gu, Y., H. Li, H. Dong, Y. Zeng, Z. Zhang, N. G. Paterson, P. J. Stansfeld, Z. Wang, Y. Zhang, W. Wang, and C. Dong, 2016. Structural basis of outer membrane protein insertion by the BAM complex. *Nature* 531:64–69.

15. Han, L., J. Zheng, Y. Wang, X. Yang, Y. Liu, C. Sun, B. Cao, H. Zhou, D. Ni, J. Lou, Y. Zhao, and Y. Huang, 2016. Structure of the BAM complex and its implications for biogenesis of outer-membrane proteins. *Nat. Struct. Mol. Biol.* 23:192–196.

16. Iadanza, M. G., A. J. Higgins, B. Schiffrin, A. N. Calabrese, D. J. Brockwell, A. E. Ashcroft, S. E. Radford, and N. A. Ranson, 2016. Lateral opening in the intact β-barrel assembly machinery captured by cryo-EM. *Nat. Commun.* 7:12865.

17. Genevrois, S., L. Steeghs, P. Roholl, J. J. Letesson, and P. van der Ley, 2003. The Omp85 protein of *Neisseria meningitidis* is required for lipid export to the outer membrane. *EMBO J* 22:1780–1789.

18. Malinverni, J. C., J. Werner, S. Kim, J. G. Sklar, D. Kahne, R. Misra, and T. J. Silhavy, 2006. YfiO stabilizes the YaeT complex and is essential for outer membrane protein assembly in *Escherichia coli*. *Mol. Microbiol.* 61:151–164.

19. Gentle, I., K. Gabriel, P. Beech, R. Waller, and T. Lithgow, 2004. The Omp85 family of proteins is essential for outer membrane biogenesis in mitochondria and bacteria. *J. Cell Biol.* 164:19–24.

20. Paschen, S. A., W. Neupert, and D. Rapaport, 2005. Biogenesis of beta-barrel membrane proteins of mitochondria. *Trends Biochem. Sci.* 30:575–582.

21. Walther, D. M., D. Rapaport, and J. Tommassen, 2009. Biogenesis of beta-barrel membrane proteins in bacteria and eukaryotes: evolutionary conservation and divergence. *Cell Mol. Life Sci.* 66:2789–2804.

22. Noinaj, N., A. J. Kuszak, J. C. Gumbart, P. Lukacik, H. Chang, N. C. Easley, T. Lithgow, and S. K. Buchanan, 2013. Structural insight into the biogenesis of β-barrel membrane proteins. *Nature* 501:385–390.

23. Albrecht, R., M. Schütz, P. Oberhettinger, M. Faulstich, I. Bermejo, T. Rudel, K. Diederichs, and K. Zeth, 2014. Structure of BamA, an essential factor in outer membrane protein biogenesis. *Acta Crystallogr. D Biol. Crystallogr.* 70:1779–1789.

24. Ni, D., Y. Wang, X. Yang, H. Zhou, X. Hou, B. Cao, Z. Lu, X. Zhao, K. Yang, and Y. Huang, 2014. Structural and functional analysis of the β-barrel domain of BamA from *Escherichia coli*. *FASEB J.* 28:2677–2685.

25. Hartmann, J. B., M. Zahn, I. M. Burmann, S. Bibow, and S. Hiller, 2018. Sequence-Specific Solution NMR Assignments of the β-Barrel Insertase BamA to Monitor Its Conformational Ensemble at the Atomic Level. *J. Am. Chem. Soc.* 140:11252–11260.

26. Wu, R., J. W. Bakelar, K. Lundquist, Z. Zhang, K. M. Kuo, D. Ryoo, Y. T. Pang, C. Sun, T. White, T. Klose, W. Jiang, J. C. Gumbart, and N. Noinaj, 2021. Plasticity within the barrel domain of BamA mediates a hybrid-barrel mechanism by BAM. *Nat. Commun.* 12:7131.

27. Noinaj, N., A. J. Kuszak, C. Balusek, J. C. Gumbart, and S. K. Buchanan, 2014. Lateral opening and exit pore formation are required for BamA function. *Structure* 22:1055–1062.

28. Lundquist, K., J. Bakelar, N. Noinaj, and J. C. Gumbart, 2018. C-terminal kink formation is required for lateral gating in BamA. *Proc. Natl. Acad. Sci. U. S. A.* 115:E7942–E7949.

29. Kim, K. H., S. Aulakh, and M. Paetzel, 2012. The bacterial outer membrane β-barrel assembly machinery. *Protein Sci.* 21:751–768.

30. van den Berg, B., 2013. Lateral gates: β-barrels get in on the act. *Nat. Struct. Mol. Biol.* 20:1237–1239.

31. Tomasek, D., S. Rawson, J. Lee, J. S. Wzorek, S. C. Harrison, Z. Li, and D. Kahne, 2020. Structure of a nascent membrane protein as it folds on the BAM complex. *Nature* 583:473–478.

32. Xiao, L., L. Han, B. Li, M. Zhang, H. Zhou, Q. Luo, X. Zhang, and Y. Huang, 2021. Structures of the β-barrel assembly machine recognizing outer membrane protein substrates. *FASEB J.* 35:e21207.

33. Höhr, A. I. C., C. Lindau, C. Wirth, J. Qiu, D. A. Stroud, S. Kutik, B. Guiard, C. Hunte, T. Becker, N. Pfanner, and N. Wiedemann, 2018. Membrane protein insertion through a mitochondrial β-barrel gate. *Science* 359:eaah6834.

34. Doyle, M. T., and H. D. Bernstein, 2019. Bacterial outer membrane proteins assemble via asymmetric interactions with the BamA β-barrel. *Nat. Commun.* 10:3358.

35. Doyle, M. T., J. R. Jimah, T. Dowdy, S. I. Ohlemacher, M. Larion, J. E. Hinshaw, and H. D. Bernstein, 2022. Cryo-EM structures reveal multiple stages of bacterial outer membrane protein folding. *Cell* 185:1143–1156.

36. Barnard, T. J., J. Gumbart, J. H. Peterson, N. Noinaj, N. C. Easley, N. Dautin, A. J. Kuszak, E. Tajkhorshid, H. D. Bernstein, and S. K. Buchanan, 2012. Molecular basis for the activation of a catalytic asparagine residue in a self-cleaving bacterial autotransporter. *J. Mol. Biol.* 415:128–142.

37. Jo, S., T. Kim, V. G. Iyer, and W. Im, 2008. CHARMM-GUI: a web-based graphical user interface for CHARMM. *J. Comput. Chem.* 29:1859–1865.

38. Wu, E. L., X. Cheng, S. Jo, H. Rui, K. C. Song, E. M. Dávila-Contreras, Y. Qi, J. Lee, V. Monje-Galvan, R. M. Venable, J. B. Klauda, and W. Im, 2014. CHARMM-GUI Membrane Builder toward realistic biological membrane simulations. *J. Comput. Chem.* 35:1997–2004.

39. Fleming, P. J., D. S. Patel, E. L. Wu, Y. Qi, M. S. Yeom, M. C. Sousa, K. G. Fleming, and W. Im, 2016. BamA POTRA Domain Interacts with a Native Lipid Membrane Surface. *Biophys. J.* 110:2698–2709.

40. Jorgensen, W. L., J. Chandrasekhar, J. D. Madura, R. W. Impey, and M. L. Klein, 1983. Comparison of simple potential functions for simulating liquid water. *J. Chem. Phys.* 79:926–935.

41. Slusky, J. S., 2017. Outer membrane protein design. *Curr. Opin. Struct. Biol.* 45:45–52.

42. Hsieh, D., A. Davis, and V. Nanda, 2012. A knowledge-based potential highlights unique features of membrane α-helical and β-barrel protein insertion and folding. *Protein Sci.* 21:50–62.

43. Ieva, R., P. Tian, J. H. Peterson, and H. D. Bernstein, 2011. Sequential and spatially restricted interactions of assembly factors with an autotransporter β domain. *Proc. Natl. Acad. Sci. USA* 108:E383–E391.

44. Feller, S. E., Y. H. Zhang, R. W. Pastor, and B. R. Brooks, 1995. Constant pressure molecular dynamics simulations — The Langevin piston method. *J. Chem. Phys.* 103:4613–4621.

45. Darden, T. A., D. M. York, and L. G. Pedersen, 1993. Particle mesh Ewald: An $N\cdot\log(N)$ method for Ewald sums in large systems. *J. Chem. Phys.* 98:10089–10092.

46. Huang, J., S. Rauscher, G. Nawrocki, T. Ran, M. Feig, B. L. de Groot, H. Grubmüller, and A. D. MacKerell, 2017. CHARMM36m: an improved force field for folded and intrinsically disordered proteins. *Nat. Methods.* 14:71–73.

47. Klauda, J. B., R. M. Venable, J. A. Freites, J. W. O'Connor, D. J. Tobias, C. Mondragon-Ramirez, I. Vorobyov, A. D. MacKerell Jr., and R. W. Pastor, 2010. Update of the CHARMM all-atom additive force field for lipids: validation on six lipid types. *J. Phys. Chem. B* 114:7830–7843.

48. Phillips, J. C., R. Braun, W. Wang, J. Gumbart, E. Tajkhorshid, E. Villa, C. Chipot, R. D. Skeel, L. Kalé, and K. Schulten, 2005. Scalable molecular dynamics with NAMD. *J. Comput. Chem.* 26:1781–1802.

49. Fiorin, G., M. L. Klein, and J. Hénin, 2013. Using collective variables to drive molecular dynamics simulations. *Mol. Phys.* 111:3345–3362.

50. Hopkins, C. W., S. Le Grand, R. C. Walker, and A. E. Roitberg, 2015. Long-Time-Step Molecular Dynamics through Hydrogen Mass Repartitioning. *J. Chem. Theory Comput.* 11:1864–1874.

51. Balusek, C., H. Hwang, C. H. Lau, K. Lundquist, A. Hazel, A. Pavlova, D. L. Lynch, P. H. Reggio, Y. Wang, and J. C. Gumbart, 2019. Accelerating Membrane Simulations with Hydrogen Mass Repartitioning. *J. Chem. Theory Comput.* 15:4673–4686.

52. Case, D. A., T. E. Cheatham, T. Darden, H. Gohlke, R. Luo, K. M. Merz, A. Onufriev, C. Simmerling, B. Wang, and R. J. Woods, 2005. The Amber biomolecular simulation programs. *J. Comput. Chem.* 26:1668–1688.

53. Humphrey, W., A. Dalke, and K. Schulten, 1996. VMD – Visual Molecular Dynamics. *J. Mol. Graphics* 14:33–38.

54. Zhang, Z., D. Ryoo, C. Balusek, A. Acharya, M. O. Rydmark, D. Linke, and J. C. Gumbart, 2021. Inward-facing glycine residues create sharp turns in β-barrel membrane proteins. *Biochim. Biophys. Acta Biomembr.* 1863:183662.

55. Danoff, E. J., and K. G. Fleming, 2015. Membrane defects accelerate outer membrane β-barrel protein folding. *Biochemistry* 54:97–99.

56. Horne, J. E., and S. E. Radford, 2022. Roll out the barrel! Outer membrane tension resolves an unexpected folding intermediate. *Cell* 185:1107–1109.